The Astrophysical Journal Letters, 741:L9 (5pp), 2011 November 1 doi:10.1088/2041-8205/741/1/L9

ON WATER FORMATION IN THE INTERSTELLAR MEDIUM: LABORATORY STUDY OF THE O + D REACTION ON SURFACES

Dapeng Jing[1], Jiao He[1], John Brucato[2], Antonio De Sio[3], Lorenzo Tozzetti[2], and Gianfranco Vidali[1]
[1] Physics Department, Syracuse University, Syracuse, NY 13244, USA
[2] INAF, Astrophysical Observatory of Arcetri, Florence, Italy
[3] Department of Astronomy & Space Science, University of Florence, Florence, Italy
Received 2011 July 18; accepted 2011 September 12; published 2011 October 10

ABSTRACT

In the interstellar medium (ISM), an important channel of water formation is the reaction of atoms on the surface of dust grains. Here, we report on a laboratory study of the formation of water via the O+D reaction network. While prior studies were done on ices, as appropriate to the formation of water in dense clouds, we explored how water formation occurs on bare surfaces, i.e., in conditions mimicking the transition from diffuse to dense clouds (Av $\sim$ 1–5). Reaction products were detected during deposition and afterward when the sample is brought to a high temperature. We quantified the formation of water and intermediary products, such as D_2O_2, over a range of surface temperatures (15–25 K). The detection of OD on the surface signals the importance of this reactant in the overall scheme of water formation in the ISM.

Key words: ISM: abundances – ISM: atoms – ISM: molecules

Online-only material: color figures

1. INTRODUCTION

Interstellar water, first detected in the microwave spectral region by Cheung et al. (1969), is found in diffuse clouds and is the main component of ices that coat dust grains in denser regions (Av > 5) of the interstellar medium (ISM). Besides its obvious role in biology, water has other important functions. In the gas phase, its abundance relative to hydrogen varies widely depending on the physical conditions of the cloud, from 10^{-8} in cold dense regions, where most is accreted on grains, to 10^{-4} in warm gas and shocked regions, where it evaporates or is sputtered from grains (Van Dishoeck & Helmich 1996; Melnick & Bergin 2005; Bjerkeli et al. 2009). When accreted on grains, it provides a medium for a rich chemistry that leads to the formation of molecules of biogenic relevance (Watanabe & Kouchi 2008; Herbst & van Dishoeck 2009); where abundant in the gas phase, it is a powerful coolant (Nisini 2000). Except for maser emissions, observations from the ground are difficult due to atmospheric water vapor. The launch of the *Herschel Space Observatory* permits to view how ubiquitous water vapor is. For example, water was detected in several envelopes of carbon stars in the asymptotic giant branch (Neufeld et al. 2011) where little was expected. Closer to home, there is much interest in understanding the source of water on planets and Kuiper Belt objects (Genda & Ikoma 2008; Encrenaz 2008).

It is now recognized that gas-phase chemistry cannot generate the amount of water that has been detected in space (d'Hendecourt et al. 1985; Hasegawa et al. 1992). It was suggested that dust grains play a role in water formation (Tielens & Hagen 1982). Although we are interested here in studying reactions involving neutral species, there are experiments that studied the formation of water by the impact of UV or cosmic ray analogs onto model ices (Ennis et al. 2011). Spurred by renewed interest in surface catalyzed reactions, there has been a flurry of theoretical and experimental works. Cuppen & Herbst (2007) and Cazaux et al. (2010) theoretically studied reaction networks leading to the formation of water. These papers also contain activation energies for key reactions. Goumans et al. (2009) calculated that if H chemisorbs on the crystalline surface of forsterite, then an oxygen atom impinging nearby would form OH. Another H atom could react with OH and form water or become chemisorbed next to OH forming a dissociated water complex. The exothermicity of the reaction can lead to the formation of H_2O.

Following Tielens & Hagen (1982), water-forming reactions on surfaces can be grouped in three main branches: reactions of H with molecular oxygen, ozone, and atomic oxygen. Miyauchi et al. (2008), Ioppolo et al. (2008), Matar et al. (2008), Oba et al. (2009), and Ioppolo et al. (2010) did experiments to study the formation of water on surfaces via the following reactions.

$$H + O_2 \rightarrow HO_2$$

$$H + HO_2 \rightarrow H_2O_2$$

$$H + H_2O_2 \rightarrow H_2O + OH$$

$$H + OH \rightarrow H_2O.$$

In these experiments, the surface is an oxygen ice laid on a metal substrate or amorphous water ice. Hydrogen atoms are made to impinge on the ice. Water as well as other products, such as H_2O_2, are detected by reflection absorption infrared spectroscopy (RAIRS; Cuppen et al. 2010). Another channel first proposed by Tielens & Hagen (1982) involves ozone:

$$O + O_2 \rightarrow O_3$$

$$H + O_3 \rightarrow O_2 + OH$$

$$H_2 + OH \rightarrow H_2O + H.$$

Mokrane et al. (2009) and Romanzin et al. (2011) looked at the formation of H_2O via this channel. Ozone was first deposited on a water ice surface, then H or D atoms were sent on this surface and the products were measured either by thermal programmed desorption (TPD; Mokrane et al. 2009) or RAIRS (Romanzin

et al. 2011). A third channel, the formation of water through successive hydrogenation of atomic oxygen,

$$H + O \rightarrow OH$$

$$OH + H \rightarrow H_2O,$$

was explored by Dulieu et al. (2010). They sent H and O beams on the surface of an amorphous water ice and detected the formation of water using TPD.

In prior experiments, water formation was studied either on model ices (such as O_2 ice) or on water ice, i.e., in simulated ISM conditions where ices are already present (Av > 4–5) and most hydrogen is in molecular form, while oxygen is poorly constrained (Caselli et al. 2010). In this study, we look at the initial stages of formation of water on grains, i.e., when atomic hydrogen and oxygen are still abundant in the gas phase, i.e., in not-so-dense regions of the ISM (Av ∼ 1–3).

2. EXPERIMENTAL

The experiments are performed in an ultra high vacuum (UHV) setup which consists of a main chamber and two molecular/atomic beamlines. Details of the setup can be found elsewhere (He et al. 2011). The sample used in the experiments is a 1 μm thick amorphous thin film of silicate deposited on a 0.5 inch diameter gold coated copper disk. The sample was prepared at the University of Florence by using a 9 kV electron beam impinging on a target consisting of MgO, FeO, and SiO_4 mixed to olivine $(MgFe)_2SiO_4$ stoichiometric ratio. The vapors from the target condensed on the disk at a rate of a few Å s^{-1}. Due to the fragility of the thin film, no ex situ cleaning of the sample is used. Instead, the sample is cleaned by repeatedly heating to 380 K in vacuum during bakeout and prior to each experiment. A triple-pass Hiden quadrupole mass spectrometer (QMS) is mounted on a rotary platform and is used to quantify the reactants entering the chamber and the products evolving from the sample surface. The two beamlines are equipped with radio-frequency (RF) dissociation sources that can generate deuterium and oxygen atoms from their parent molecules. D_2 and $^{18}O_2$ are used to distinguish their molecular and atomic species from their native counterparts in the chamber.

There are two distinct phases of the experiments: the exposure phase and the desorption phase. In a typical experiment, the sample is kept at a desired temperature (usually 10–30 K) and is simultaneously exposed to deuterium and oxygen beams. After the desired exposure time, the beam flux is cut off and the sample temperature is raised to desorb various species on the surface. The QMS detector is placed in front of the sample to detect the composition of gases evolving from the sample in both phases of the experiment. Water formation is also monitored using RAIRS. A spectral resolution of 2 cm^{-1} is used and 256 scans are co-added.

The beam composition and flux are measured by placing the QMS detector directly in sight with the beam. In unit time, the ratio of the number of molecules entering the detector to the counts generated is obtained by flooding the main chamber with the desired gases (D_2 and O_2), where the exact number density of molecules in the chamber can be calculated from the chamber pressure. Gas correction factors for D_2 of 0.35 and O_2 of 1.0 are used since the ionization gauge is calibrated for N_2. When the RF sources are turned on, the deuterium beam has a dissociation efficiency of 67% and the oxygen beam of 48%. The calculated D flux is 1.5×10^{13} cm^{-2} s^{-1}, D_2 flux is 3.7×10^{12} cm^{-2} s^{-1}, O flux is 2.8×10^{12} cm^{-2} s^{-1}, and O_2 flux is 1.5×10^{12} cm^{-2} s^{-1}. We also measure traces of various masses to determine the composition of the beams. Except for $H_2{}^{16}O$ from the background of the beamline chambers, no other contamination species (N_2, $^{16}O_2$, NO, and CO_2) are found.

Table 1
Formation Slopes and Efficiencies of Various Products

Slope and Efficiency ε	HDO	D_2O	D_2O_2	O_3
15 K slope (cm^{-2} $minute^{-1}$)	1.5×10^{13}	4.2×10^{13}	7.6×10^{13}	2.6×10^{12}
25 K slope (cm^{-2} $minute^{-1}$)	1.2×10^{13}	3.0×10^{13}	8.9×10^{13}	4.9×10^{12}
ε at 15 K	0.043	0.12	0.22	0.007
ε at 25 K	0.034	0.087	0.26	0.014

3. RESULTS AND DISCUSSION

In this section, we present our experimental results in detail. First, we expose the sample to D and O atoms simultaneously at 15 K and 25 K. TPD results clearly show the formation of water (HDO and D_2O) as well as D_2O_2 and O_3. The presence of HDO is not surprising although only D is used. It is known that during heating, an isotope exchange between water molecules will occur (Smith et al. 1997). This is also observed by Dulieu et al. (2010).

As shown in Figure 1, mass spectra of HDO show a typical zeroth-order desorption kinetics with a shared leading edge and highly asymmetric peaks leaning to the right. This corresponds to the sublimation of physisorbed HDO molecules weakly bounded to the substrate. D_2O peaks also share the leading edge. However, the peak shape is not as asymmetric as HDO peaks. This could arise from the lateral interaction through hydrogen bonding between D_2O molecules (Sanchez 1996). Intermediary products, such as D_2O_2 and O_3, are also observed as indicated by the peaks of mass 40 and 54 at around 180 K and 60 K, respectively. The TPD data are then applied to a simple rate equation model (Perets et al. 2007). The number of molecules of a certain species on the surface N can be expressed by the following formula:

$$-dN/dt = \nu \exp(-E_d/k_B T),$$

where E_d is the desorption energy, T is the surface temperature, k_B is the Boltzmann constant, and ν is the attempt rate which is taken to be 10^{12} s^{-1}. We estimated the desorption energy for various species to be $(3.9 \pm 0.2) \times 10^2$ meV for HDO, $(4.0 \pm 0.2) \times 10^2$ meV for D_2O, $(4.3 \pm 0.3) \times 10^2$ meV for D_2O_2, and $(1.7 \pm 0.1) \times 10^2$ meV for O_3. Note that our results are significantly higher compared to what has been reported by Cuppen & Herbst (2007)—172 meV for H_2O and 229 meV for H_2O_2 on graphite. However, a strong dependence of desorption energy on substrate material is expected. A desorption energy of 632 meV for water on MgO(1 0 0) surface has been reported by Günster et al. (2000).

Our results also show a linear formation of water and D_2O_2 as a function of D and O fluencies in the exposure time range of our study (see Figure 2). The slope in units of column density per exposure time is shown in Table 1. The column density is estimated from the integrated desorption peak area. The conversion factor from TPD peak area to column density is obtained from a calibration experiment in which $D_2{}^{16}O$ vapor is deposited on the sample from one beamline and then desorbed using TPD. The amount of $D_2{}^{16}O$ deposited can be accurately calculated from beam flux and related to the TPD peak area to

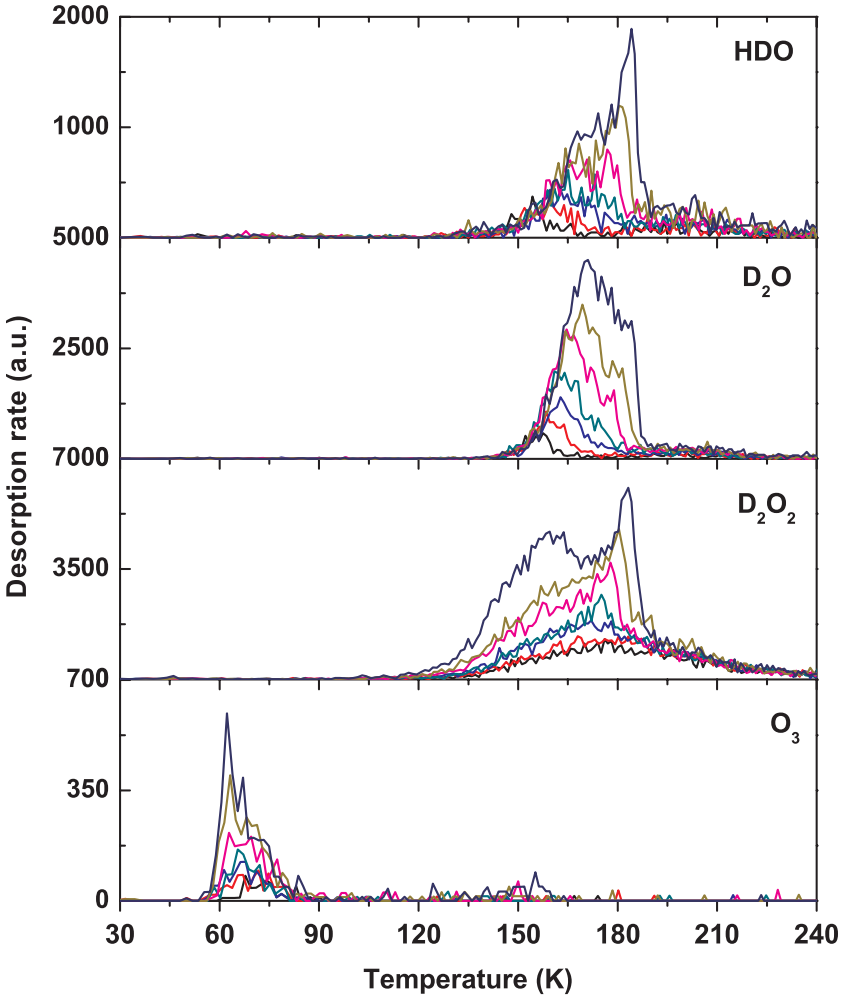

Figure 1. Desorption peaks for various species after D and O co-exposure at 15 K. From bottom to top: 10 minutes, 15 minutes, 22.5 minutes, 30 minutes, 45 minutes, 60 minutes, and 90 minutes.

(A color version of this figure is available in the online journal.)

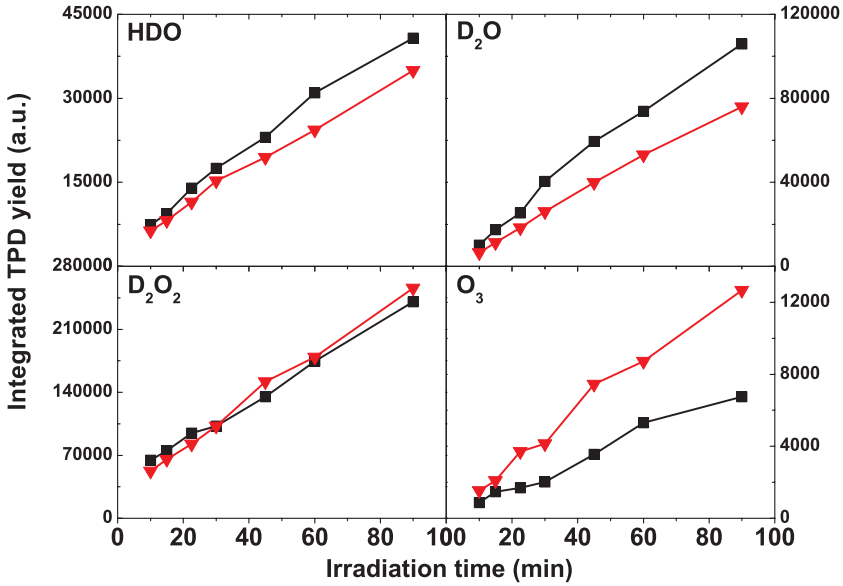

Figure 2. Integrated TPD yield of various species as a function of exposure time for D and O co-exposure at 15 K (squares) and 25 K (triangles).

(A color version of this figure is available in the online journal.)

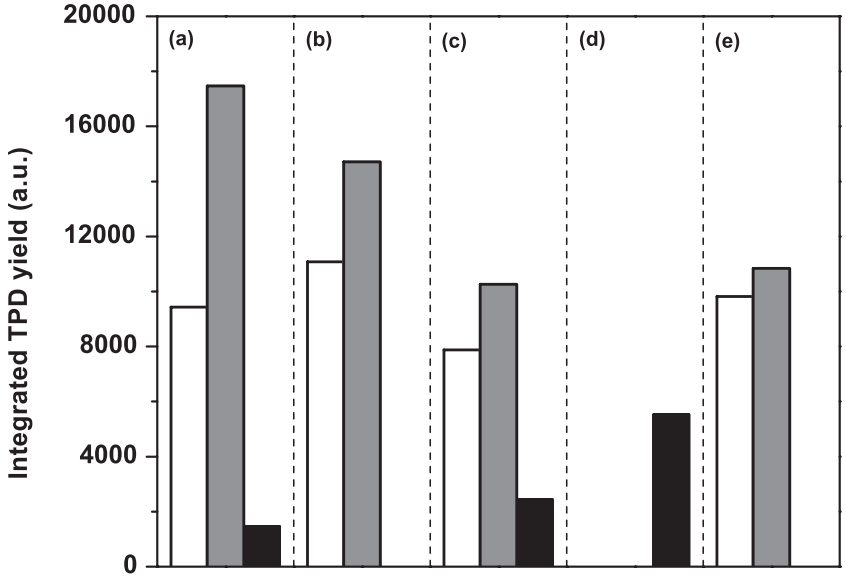

Figure 3. Bar plots of integrated TPD yield of various species for different scenarios of exposures at 15 K. White: HDO, gray: D_2O and black: O_3. (a) 15 minute D and O co-exposure; (b) 15 minute D and O_2 co-exposure; (c) 15 minute O then 15 minute D exposure; (d) 15 minute D then 15 minute O; and (e) 15 minute O_2 then 15 minute D.

get the conversion factor. Note that in the slope calculations, we make the reasonable assumption that for our QMS detector, $HD^{18}O$, $D_2{}^{18}O$, $D_2{}^{18}O_2$, and $^{18}O_3$ have the same ionization efficiency as $D_2{}^{16}O$. As shown in Figure 2, more water (HDO and D_2O) is produced when the temperature is reduced from 25 K to 15 K. The amount of D_2O_2 does not seem to be affected by the surface temperature. The linear formation of products can also be expressed in terms of constant formation efficiency ε of various species. ε is expressed by the ratio of the oxygen nuclei in the product to the oxygen nuclei from the beam (including both O and O_2) and is also shown in Table 1. Our observations of formation of D_2O and D_2O_2 are similar to what has been obtained by Ioppolo et al. (2010). They found an initial linear and temperature-independent formation of both D_2O and D_2O_2. The relative amount of water produced with respect to D_2O_2 is also similar to their results.

In Figure 3, we show the yields of products obtained in different experiments. The yields are calculated by integrating the TPD traces (see Figure 1). A few comments can be made. First, atomic D deposition on clean surface (D first) does not produce any water species at 15 K. This is probably due to the recombination of D atoms into D_2 in the absence of oxygen. Since $D + D \rightarrow D_2$ has no activation barrier and diffusion of D atoms on clean surface is easily achieved (Cuppen & Herbst 2007). Second, we observe that D_2O formation is accompanied with the detection of HDO. Examining Figure 3, HDO formation is roughly constant across different types of experiments (panels (a)–(e)). On the other hand, the D_2O yield changes more pronouncedly. The sum of the HDO and D_2O yields is approximately constant in the co-exposure measurements, but higher than the sequential measurements. At this time, it is not clear what dictates the relative weights of HDO and D_2O. More experiments will be necessary to clarify this point. Third, by looking at Figure 2, we see that less O_3 is desorbed for lower temperature exposure. We think that this is due to the competition among different processes. Ozone is produced via the combination of O and O_2. At higher temperature, there are less D atoms on the surface to react with O atoms. Therefore, more O atoms react with O_2 to make O_3. Our observation of less amount of O_3 desorbed with decreasing surface temperature seems to contradict the results from Sivaraman et al. (2007). However, one should note that in their experiments, O_3 is produced by electron irradiation on O_2 ice, whereas in our experiments, O and O_2 coexist in the beam and arrive on the surface at the same time.

We now turn to qualitative in situ RAIRS measurement since TPD does not allow to distinguish between products formed during exposure and during heating. Here we should point out that the substrate in the experiment is an amorphous film of silicate, which has a black, opaque finish. The infrared beam reflects poorly on this surface. Therefore, our RAIRS measurements suffer from high detection limit and low signal strength. Nonetheless, we managed to obtain IR data from an extended exposure experiment. In the RAIRS experiment, the change in absorbance (ΔA) with respect to the clean surface is acquired every hour during a 5 hr D and O co-exposure. The ΔA spectra are shown in Figure 4. The double peak at around 2360 cm^{-1} and 2335 cm^{-1} is due to CO_2 gas in the IR detector housing which is outside of the UHV chamber. The narrow peak at 2307 cm^{-1} is attributed to substrate–OD stretching vibration absorption. The broad peak centered at around 2400 cm^{-1} is attributed to the overlapping of D_2O and D_2O_2 O–D stretching. The smaller peak centered at 2100 cm^{-1} is attributed to D_2O_2 $2\nu_6$ mode. Peaks at around 1207 cm^{-1} and 1050 cm^{-1} are attributed to D_2O and D_2O_2 O–D bending. The 2100 cm^{-1} peak is clear evidence for D_2O_2 formation during exposure. The strong adsorption peak at 2300 cm^{-1} shows an abundance of OD radicals on the surface, which explains the robust formation of D_2O_2 via $OD + OD \rightarrow D_2O_2$ reaction route. The evidence for D_2O formation during exposure is the small peak at 1207 cm^{-1} clearly shown for the 5 hr curve.

Finally, in the experiments described above, we measured for the first time the initial stages of formation of water on amorphous silicates as they are thought to occur in not-so-dense ISM environments. We have shown the importance of the formation of OD and quantified the efficiencies of the various reactions. Because of experimental constraints, in particular the unavoidable mixture of O and O_2, the further disentanglement

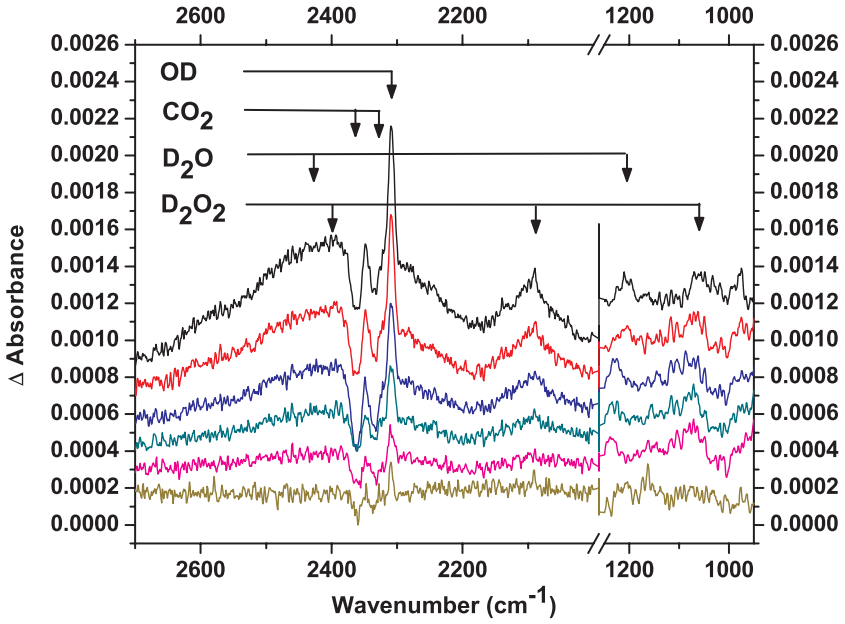

Figure 4. RAIR spectra of D and O co-exposure at 15 K for (from bottom to top) 15 minutes, 1 hr, 2 hr, 3 hr, 4 hr, and 5 hr.
(A color version of this figure is available in the online journal.)

of various reaction pathways requires more experiments and the setting up of a system of rate equations to, first, obtain more information from the experimental results, and, second, to take these results and use them in simulations of molecule formation in actual ISM conditions. Such work is now in progress and will be reported later.

This work is supported by the NSF, Astronomy & Astrophysics Division (grant No. 0908108), and by MIUR PRIN-08. We thank Dr. Paul Frank for assistance in preliminary experiments.

REFERENCES

Bjerkeli, P., Liseau, R., Olberg, M., et al. 2009, A&A, 507, 1455
Caselli, P., Keto, E., Pagani, L., et al. 2010, A&A, 521, L29
Cazaux, S., Cobut, V., Marseille, M., Spaans, M., & Caselli, P. 2010, A&A, 522, A74
Cheung, A. C., Rank, D. M., Townes, C. H., Thornton, D. D., & Welch, W. J. 1969, Nature, 221, 626
Cuppen, H. M., & Herbst, E. 2007, ApJ, 668, 294
Cuppen, H. M., Ioppolo, S., Romanzin, C., & Linnartz, H. 2010, Phys. Chem. Chem. Phys., 12, 12077
d'Hendecourt, L. B., Allamandola, L. J., & Greenberg, J. M. 1985, A&A, 152, 130
Dulieu, F., Amiaud, L., Congiu, E., et al. 2010, A&A, 512, A30
Encrenaz, T. 2008, ARA&A, 46, 57
Ennis, C., Bennett, C. J., Jones, B. M., & Kaiser, R. I. 2011, ApJ, 733, 79
Genda, H., & Ikoma, M. 2008, Icarus, 194, 42
Goumans, T. P. M., Catlow, C. R. A., Brown, W. A., Kastner, J., & Sherwood, P. 2009, Phys. Chem. Chem. Phys., 11, 5431
Günster, J., Liu, G., Stultz, J., Krischok, S., Goodman, D. W., et al. 2000, J. Phys. Chem. B, 104, 5738
Hasegawa, T. I., Herbst, E., & Leung, C. M. 1992, ApJS, 82, 167
He, J., Frank, P., & Vidali, G. 2011, Phys. Chem. Chem. Phys., 13, 15803
Herbst, E., & van Dishoeck, E. F. 2009, ARA&A, 47, 427
Ioppolo, S., Cuppen, H. M., Romanzin, C., van Dishoeck, E. F., & Linnartz, H. 2008, ApJ, 686, 1474
Ioppolo, S., Cuppen, H. M., Romanzin, C., van Dishoeck, E. F., & Linnartz, H. 2010, Phys. Chem.. Chem. Phys., 12, 12065
Matar, E., Congiu, E., Dulieu, F., Momeni, A., & Lemaire, J. L. 2008, A&A, 492, L17
Melnick, G. J., & Bergin, E. A. 2005, Adv. Space Res., 36, 1027
Miyauchi, N., Hidaka, H., Chigai, T., et al. 2008, Chem. Phys. Lett., 456, 27
Mokrane, H., Chaabouni, H., Accolla, M., et al. 2009, ApJ, 795, L195
Neufeld, D. A., González-Alfonso, E., Melnick, G., et al. 2011, ApJ, 727, L29
Nisini, B. 2000, Science, 290, 1513
Oba, Y., Miyauchi, N., Hidaka, H., et al. 2009, ApJ, 701, 464
Perets, H. B., Lederhendler, A., Biham, O., et al. 2007, ApJ, 661, L163
Romanzin, C., Ioppolo, S., Cuppen, H. M., van Dishoeck, E. F., & Linnartz, H. 2011, J. Chem. Phys., 134, 084504
Sanchez, J. R. 1996, Langmuir, 12, 36
Sivaraman, B., Jamieson, C. S., Mason, N. J., Kaiser, R. I., et al. 2007, ApJ, 669, 1414
Smith, S. R., Huang, C., & Kay, B. D. 1997, J. Phys. Chem. B, 101, 6123
Tielens, A. G. G. M., & Hagen, W. 1982, A&A, 114, 245
Van Dishoeck, E. F., & Helmich, F. P. 1996, A&A, 315, L177
Watanabe, N., & Kouchi, A. 2008, Prog. Surf. Sci., 83, 439